SWIRLS 3D CE-MRA with Field-Corrected Sparse SENSE Reconstruction

Joshua D. Trzasko[1], Yunhong Shu[1], Armando Manduca[1], John Huston III[1], and Matt A. Bernstein[1]
[1]*Mayo Clinic, Rochester, MN, United States*

TARGET AUDIENCE: Image reconstruction developers and users of non-Cartesian sequences for MR angiography.

PURPOSE: SWIRLS is a centrically-ordered 3D spherical non-Cartesian trajectory that has shown promise for contrast-enhanced magnetic resonance angiography (CE-MRA) [1]. As previously demonstrated [2], the incoherency of the SWIRLS sampling operator also makes this acquisition method well-suited for sparsity-driven image reconstruction. In this work, we describe a sparse reconstruction framework for SWIRLS 3D CE-MRA reconstruction that additionally incorporates sensitivity encoding (SENSE) [3] and accounts for susceptibility-induced off-resonance, which can confound visualization of vasculature near the sinus cavities. We then demonstrate the performance benefit obtained by migrating from the current "gridding" protocol to this generalized reconstruction framework.

METHODS: Under an IRB-approved protocol and after obtaining written consent, 3 patients were scanned at 3T (GE, DVMR 20.1IB, Milwaukee, WI) using a 3.35x undersampled SWIRLS acquisition (FOV = 24 cm, TR = 7.4 ms, BW = ±62.5 kHz, FA = 35^{o}, 8047 shots, 512 samples/shot, 8-channel head coil, Duration = 1:00). A 2 mL test bolus was used for timing fluoroscopy. A 12 mL bolus of gadobenate dimeglumine contrast (Multihance, Bracco Diagnostics, Princeton, NJ) was injected into the right antecubital vein at 3 mL/s, followed by a power-injected 50 mL saline flush. Additionally, a dual-echo 3D GRE calibration scan (FOV = 24 cm, TR = 9.5 ms, TE = 3.9/6.2 ms, BW = ±62.5 kHz, FA = 10^{o}, Matrix = 256x128x60, Duration = 2:44) was performed. From the calibration scan, a B_0 field map estimated using a multi-channel generalization of Funai et al.'s regularized strategy [4]. Receiver sensitivity profiles were then estimated from this same data set using the variational strategy in [5]. Image reconstruction was performed via both coil-by-coil gridding with Voronoi density compensation and by the following penalty regression: $[\hat{u}] = \arg\min \alpha P(u) + \|A(\omega)Su - g\|_2^2$, where *u* is the target image, *g* is the multi-channel k-space data, *S* is the set of sensitivity profiles, ω is the B_0 field map, *A* is a forward operator. Following the Gauss-Markov theorem, we highlight that no density compensation is used within this model. When ignoring off-resonance (ω=0), *A* was realized via a 1.25x oversampled non-uniform fast Fourier transform (NUFFT) [6] employing a *J*=5 Kaiser-Bessel kernel [7]. When accounting for off-resonance, *A* was constructed using the aforementioned NUFFT and time-segmented approximation [8,9] employing *L*=8 segments and a Hann window. All reconstructed volumes were of dimension 240^3. Additionally, the penalty functional, *P*, was assigned for both Tikhonov ($P(u) = \|u\|_2^2$) and wavelet sparse ($P(u) = \|\Psi u\|_1$) regression. The sparsifying transform, ψ, was implemented as the 4-tap 3D Daubechies wavelet using the lifting scheme [10]. The regularization parameter was manually selected as α=1e-10 and α=2.5e-5 for Tikhonov and sparsity regression, respectively. In all cases, (1) was solved using FISTA [11] (iterations = 100, Lipschitz constant estimated via power iteration); wavelet random shifting [12] was also employed for sparse regression to mitigating blocking artifacts. All reconstructions were implemented in C++ using FFTW and OpenMP, and executed on a dual 6-core (Intel x5670, 2.93 GHz, 12 MB cache) machine with 24 GB DDR3 1333 MHz memory.

RESULTS: Figure 1 shows 25 mm thin-slab maximum intensity projections (MIPs) at the level of the Circle of Willis for an example set of results obtained for a single volunteer. Results of standard gridding, Tikhonov regression (SENSE), and sparse regression (SPARSE-SENSE) reconstruction executed with and without handling of off-resonance effects are shown. As expected, within all paradigms accounting for off-resonance effects mitigates geometric distortion near high susceptibility areas like the nasal sinus. Migrating from gridding to standard SENSE (Tikhonov) reconstruction, noise is markedly reduced without compromise of structure information. The noise reduction results both from the avoidance of density compensation and improved statistical efficiency from sensitivity encoding. Additional utilization of the sparsity penalty acts to further suppress noise amplification and improve vessel-to-tissue contrast.

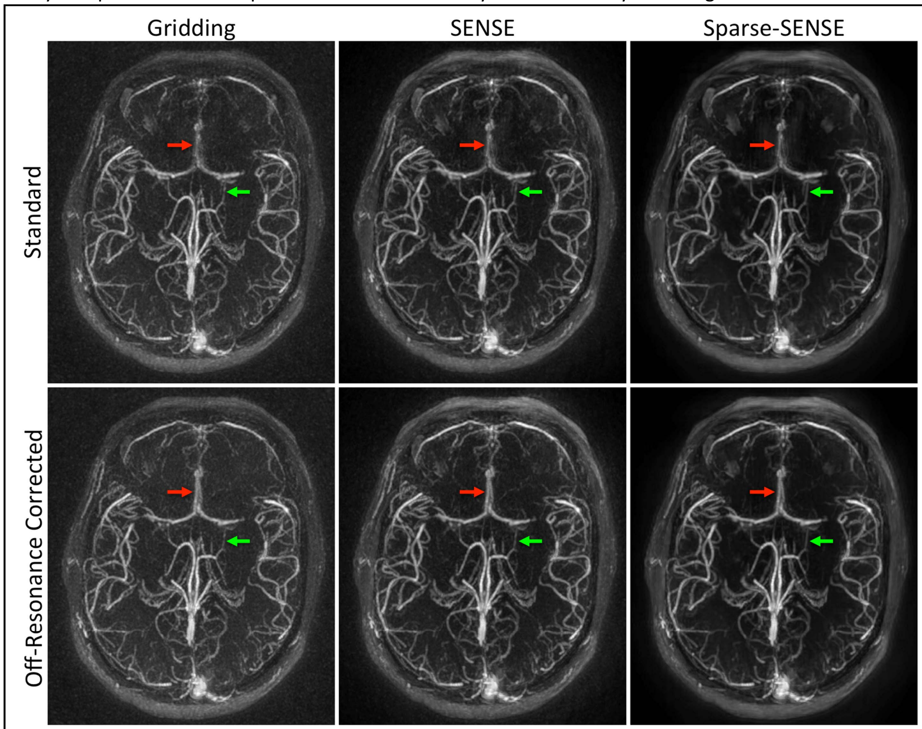

FIG 1: 25 mm thin-slab MIPs for different reconstructions of a 3.35x undersampled SWIRLS CE-MRA. Note the distortion of the anterior cerebral arteries (red) in reconstructions that do not account for off-resonance, as well as the reduction in noise and improvement in small vessel conspicuity (green) when migrating from gridding to SENSE to Sparse-SENSE. Images are identically windowed and levels.

DISCUSSION: The results in Figure 1 highlight the complimentary gains in reconstruction performance for SWIRLS 3D CE-MRA that can be obtained by utilizing off-resonance correction, sensitivity encoding, and sparsity, as compared to the conventional gridding reconstruction strategy. However, the high computational expense of the advanced strategies – 30 min for (Sparse-)SENSE without, or 200 min with, off-resonance correction – is clinically prohibitive, and further work is needed to reduce reconstruction time. Potential pathways for achieving such reduction include development of alternative optimization routines and adoption of advanced hardware platforms.

CONCLUSION: Sensitivity encoding, sparsity, and off-resonance correction provide complementary gains in image quality for SWIRLS 3D CE-MRA by mitigating noise amplification and geometric distortion.

REFERENCES: [1] Y. Shu et al., ISMRM 2011:2656; [2] J. Trzasko et al., ISMRM 2012:4208; [3] K. Pruessmann et al., MRM 46:638-51, 2001; [4] A. Funai et al., IEEE TMI 27:1484-94, 2008; [5] S. Keeling and R. Bammer, Appl. Math. Comp. 158:53-82, 2004; [6] J. Fessler and B. Sutton, IEEE TSP 51:560-64, 2003; [7] P. Beatty et al., IEEE TMI 24:799-808, 2005; [8] D. Noll et al., IEEE TMI 10:629-37, 1991; [9] B. Sutton et al., IEEE TMI 22:178-88, 2003; [10] I. Daubechies and W. Sweldens, J. Fourier Anal. Appl. 4:247-69, 1998; [11] A. Beck and M. Teboulle, SIAM Imag. Sci. 2:183-202, 2009; [12] M. Guernquin-Kern et al., IEEE TMI 30:1649-60, 2011.